Optimal operating conditions and configurations for humidification-dehumidification desalination cycles

Karan H. Mistry[a], Alexander Mitsos[a], John H. Lienhard V[a,*]

[a]*Department of Mechanical Engineering, Massachusetts Institute of Technology, Cambridge, MA, USA*

Abstract

This article applies nonlinear programming techniques to optimize humidification-dehumidification (HD) desalination cycles for operating conditions that result in maximum gained output ratio (GOR). Closed air open water as well as open air open water cycles, each with either an air or a water heater, were considered in this analysis. Numerical optimization resulted in a substantial increase in GOR for all four cycle types compared to previous best-case conditions found using heuristic studies. The GOR of the cycles was found to decrease with increasing component terminal temperature difference (TTD). In addition, different cycles perform best at different temperature differences. Optimization also revealed that some counterintuitive design configurations can result in superior performance under the appropriate operating conditions.

Keywords: humidification-dehumidification, desalination, numerical optimization, nonlinear programming, cycle optimization

*Corresponding author
Email address: lienhard@mit.edu (John H. Lienhard V)

Nomenclature

Roman Symbols

c_p	specific heat capacity at constant pressure [kJ/kg-K]
f	objective function
$\mathbf{g}$	vector of constraints
$\dot{H}$	enthalpy flow rate [kW]
h	specific enthalpy (per kg dry air for moist air, per kg water for liquid water) [kJ/kg]
h_{fg}	enthalpy of vaporization (per kg distillate) [kJ/kg]
L	length of heater [m]
$\dot{m}$	mass flow rate [kg/s]
m_r	mass flow rate ratio (feed water to dry air) [-]
p	pressure [kPa]
$\dot{Q}_{in}$	heat input [kW]
$\dot{S}_{gen}$	entropy generation rate [kW/K]
s	specific entropy (per kg dry air for moist air, per kg water for liquid water) [kJ/kg-K]
s_{gen}	Specific entropy generation (per kg product) [kJ/kg-K]
ΔT	temperature difference from heater surface to fluid bulk temperature [K]
T	temperature [K]
$\mathbf{x}$	vector of optimization variables
x	axial coordinate along length of heater [m]

Greek Symbols

ϵ	component effectiveness [-]
ω	humidity ratio, mass basis [kg water vapor/kg dry air]

Superscripts

L	lower bound
U	upper bound

Subscripts

a	dry air, air stream
b	bulk property
D	dehumidifier
d	destroyed
f	saturated liquid
H	humidifier
h	fluid in heater
HT	heater
$ideal$	ideal condition
in	inlet
max	maximum system temperature
out	outlet
p	product/condensate
$total$	sum of all components
$trans$	transferred
w	seawater, water stream
$wall$	heated surface
WB	wet bulb
0	ambient conditions

Acronyms

AH	air heated

CAOW	closed air, open water
GOR	gained output ratio [-]
HD	humidification dehumidification
OAOW	open air, open water
TTD	terminal temperature difference [K]
WH	water heated

1. Introduction

Several excellent methods of desalination are available, including reverse osmosis (RO), multi-stage flash (MSF), and multi-effect distillation (MED), but these technologies are often unsuitable for developing regions because they require substantial infrastructure, typically use fossil fuels as the energy source, and may only be cost-effective at very large scales. Conversely, many areas that suffer from water scarcity have high solar insolation, which suggests that solar powered desalination could be very beneficial to the developing world since the sun provides an abundance of "free" energy.

Humidification-dehumidification (HD) desalination is a fairly simple technology that mimics nature's water cycle and has the potential to operate with solar heating. Solar stills are the most basic form of HD but prove to be inefficient since the enthalpy of vaporization is lost in the condensation process [1]. The basis of HD desalination cycles is to improve system efficiency by recapturing this energy, by separating the evaporation and condensation processes, and by incorporating regenerative heating of the feedwater stream in the condenser. Due to the straightforward design and the potential for production of potable water in remote areas without the need for electricity, HD has received considerable attention over the past few years [1–3].

Previous studies by Narayan et al. [4] and by Mistry et al. [5] investigated the thermodynamic behavior of HD cycles using the First and Second Laws, respectively. Both articles discussed methods for improvement and optimization of the cycles based on thermodynamic arguments and single parameter optimization. However, the cycles are functions of several parameters and therefore, more systematic optimization methods are required to find the true optimal conditions for each of the cycles. The goal of this paper is to determine operating conditions that maximize the gained output ratio (GOR), or performance ratio, of a variety of promising HD cycles. Three numeric codes (SNOPT [6, 7], Interior Point Optimizer (IPOPT) [8], and an in-house genetic

algorithm) were used to perform the optimization. A multistart method was also used for heuristic global optimization, implemented in parallel computers in order to reduce computation time.

2. HD Desalination Cycles

HD cycles must consist of at least three components: a humidifier, a dehumidifier, and a heater. Depending on how these three components are arranged, various classes of cycles can be formed. The cycles are classified based on the nature of the flow pattern of each of the streams. Two primary cycle classes are considered here: closed air, open water (CAOW) cycles and open air, open water (OAOW) cycles.

The characteristics of these basic cycles are discussed below.

2.1. Closed Air, Open Water (CAOW) HD Cycles

The CAOW cycle is one of the most basic forms of an HD cycle and was analyzed using the First Law by Narayan et al. [4]. This cycle can be driven by either a water heater or an air heater, thus forming two distinct configurations. The closed air, open water, water heated (CAOW-WH) cycle is shown in Fig. 1 and the closed air, open water, air heated (CAOW-AH) cycle is shown in Fig. 2. The water heated cycle is considered first.

2.1.1. Closed Air, Open Water, Water Heated (CAOW-WH) Cycles

[Figure 1 about here.]

[Figure 2 about here.]

In this cycle, seawater enters the system at the dehumidifier and is used to cool and dehumidify a warmer, moist air stream. In the associated condensation process, the enthalpy of vaporization is transferred from the moist air to the seawater, thus warming

the feed stream. The condensate is removed as product water and the seawater is then further heated in a heater (potentially a solar heater).

The hot seawater is then used to humidify a cooler air stream and the remaining seawater is extracted as brine. In the evaporation process, heat and mass is transferred from the hot seawater stream to the moist air stream. In this configuration, the air stream continuously circulates between the humidifier and the dehumidifier.

2.1.2. Closed Air, Open Water, Air Heated (CAOW-AH) Cycles

A second form of the closed air, open water cycle can be achieved by removing the (solar) heater from the water stream and adding one to the air stream as shown in Fig. 2. This cycle is known as a closed air, open water, air heated (CAOW-AH) cycle.

Both the air and water streams follow the same flow path through the humidifier and dehumidifier, as in the CAOW-WH cycle. However, instead of heating the water stream, the heater is now placed in the air stream. There are two possible locations in the air stream for the heater: before the humidifier and before the dehumidifier. Placing the heater prior to the humidifier results in better cycle performance as discussed by both Narayan et al. [4] and Mistry et al. [5].

2.2. Open Air, Open Water (OAOW) HD Cycles

Two additional cycle configurations can be formed by breaking the connection in the air stream between the humidifier and dehumidifier (between points 5 and 8 in Figs. 1 and 2). When this is done, an open air, open water (OAOW) cycle is formed, since the air stream now makes a single pass through the system. As with the closed air cycles, the open air cycles can be either water heated (OAOW-WH, Fig. 3) or air heated (OAOW-AH, Fig. 4).

[Figure 3 about here.]

[Figure 4 about here.]

These cycles operate in a very similar fashion to their closed air counterparts. However, it is important to note that the open air cycles are heavily dependent upon the ambient conditions since the air stream is taken directly from the environment. Therefore, it should be expected that the performance of the OAOW cycles will fluctuate as the ambient temperature and relative humidity vary.

3. Models and Simulations

3.1. Modeling Methodology

The initial modeling effort for these HD cycles was performed using Engineering Equation Solver (EES) [9] as discussed in [5]. While EES was very useful for the initial phase of HD analysis, the current effort to optimize over a large number of parameters required more sophisticated numerical methods than available in EES. Various software packages were considered for the analysis, but ultimately, JACOBIAN [10] was selected. JACOBIAN simplifies the modeling of more complicated process configurations through its modular method of model development. Complicated system models are built up by first modeling smaller components and then combining the component models to form a complete system. Modular development of systems allows for much cleaner models that are easier to modify while studying variations of a given system.

Most importantly, an existing computational infrastructure linking various optimization solvers to JACOBIAN could be exploited. These optimization codes (discussed below) are much more sophisticated than what is available in EES and allow for more customization of the optimization process as well as optimization over a greater number of parameters.

The model presented in this paper implements the same equations used by Mistry et al. [5], but is divided into individual component models. Both models result in

nearly identical results with slight differences occurring as a result of minor difference in physical property implementations.

3.2. Approximations

In this analysis, several standard approximations are made. First, all calculations are performed for steady state at atmospheric pressure. Kinetic and potential energy effects are neglected and pumping power is assumed to be negligible compared to heat input since these effects are orders of magnitude smaller. Second, the humidifier and dehumidifier are taken to be adiabatic with respect to the environment. This can be achieved with proper insulation. Third, the moist air streams are taken to be saturated at the exit of both the humidifier and the dehumidifier. Approximately saturated air at the exit is readily achieved when both components are properly designed and have sufficient contact area. Finally, the dehumidifier condensate bulk temperature is evaluated as a function of the inlet and outlet wet-bulb temperatures of the moist air using a model discussed in [5].

Seawater physical properties are approximated by pure water properties. General cooling tower design practice shows that physical properties, such as the vapor pressure, vary by about 1% per $10,000$ ppm salinity [11–13].

3.3. Fluid Properties

Property data for dry air, liquid water, water vapor, and moist air were programmed using formulations from the literature since JACOBIAN does not have built in packages for these. Dry air is modeled as an ideal gas according to the formulations presented by [14]. The model was verified by comparing to REFPROP [15].

Liquid water properties are evaluated using the International Association for the Properties of Water and Steam's 1997 Industrial Formulation [16]. The water property model was also verified by comparing to REFPROP.

Moist air properties are evaluated by summing the mass-weighted properties of the constituent substances (ideal solution assumption). Moist air properties were verified by comparing to the values found in the ASHRAE Fundamentals Handbook [17], which is based on the work of Hyland and Wexler [18].

3.4. HD Components

The governing equations for each of the humidifier, dehumidifier, and heater are summarized below.

3.4.1. Humidifier and Dehumidifier

[Figure 5 about here.]

Humidifiers and dehumidifiers are simultaneous heat and mass exchangers with similar governing equations. Figure 5 shows humidifier and dehumidifier control volumes with inlet and outlet flows. The water leaving the humidifier is also referred to as brine. Approximating the humidifier and dehumidifier as adiabatic, the First and Second Laws are written for each as follows:

$$0 = \sum_{out} \dot{m}_{out} h_{out} - \sum_{in} \dot{m}_{in} h_{in} \quad (1)$$

$$\dot{S}_{gen} = \sum_{out} \dot{m}_{out} s_{out} - \sum_{in} \dot{m}_{in} s_{in} \quad (2)$$

Assuming that the two inlet temperatures are known, and that the dehumidifier condensate temperature can be evaluated as a function of the inlet and outlet moist air stream wet-bulb temperature, there are three unknowns (outlet moist air temperature, water temperature, and entropy generation) but only two equations, (1) and (2). Therefore, an additional equation is needed. The effectiveness of the humidifier and dehumidifier is introduced to completely define the component inlet and outlet states.

The effectiveness of the humidifier and dehumidifier is calculated in a similar fashion as effectiveness is calculated for a two stream heat exchanger. In the latter case, effectiveness is defined as the actual heat transfer divided by the theoretical maximum heat transfer, $C_{min}\,(T_{hot,in} - T_{cold,in})$, where C_{min} is the minimum heat capacity rate of the two streams. The mass transfer between the air and water streams in the present case makes the stream enthalpy change (a function of temperature and humidity) the natural variable upon which to focus. Therefore, an energy-based method of calculating the effectiveness is formulated [19, 20]. First, the effectiveness is calculated in two ways — assuming the water stream has the lower maximum enthalpy change, ϵ_w, and then assuming the air stream has the lower maximum enthalpy change, ϵ_a:

$$\epsilon_w = \frac{\Delta \dot{H}_w}{\Delta \dot{H}_{w,ideal}}, \qquad \epsilon_a = \frac{\Delta \dot{H}_a}{\Delta \dot{H}_{a,ideal}} \tag{3a}$$

The two ideal enthalpy changes are evaluated assuming a zero terminal temperature difference at the top (or bottom) of the exchanger: $T_{w,out,ideal} = T_{a,in}$ and $T_{a,out,ideal} = T_{w,in}$. Additionally, the moist air stream is assumed to be saturated ($\phi = 1$) at the exits.

Note that the numerators of Eq. (3a) are equal, by the First Law (in the dehumidifier, $\Delta \dot{H}_a$ includes the moist air and condensate). Additionally, the stream with the lower total capacity rate will have a smaller ideal enthalpy change. Therefore, the actual effectiveness, ϵ, will always be the greater of the two values in Eq. (3a):

$$\epsilon = \max\left(\epsilon_w, \epsilon_a\right) \tag{3b}$$

Both ϵ_w and ϵ_a must be calculated since it is not known a priori which one is larger.

Under this definition of the component effectiveness, it is not always possible to achieve one hundred percent effectiveness without producing unobtainable temperature

crossovers between the streams, which would violate the Second Law. This situation is similar to the inability of parallel flow heat exchangers to reach one hundred percent effectiveness for some capacity rate ratios [19, 20]. To address this issue, at least partially, a constraint was imposed in the optimization calculations requiring that entropy generation was always greater than zero.

To fully define the dehumidifier, a relationship between the condensate temperature and the inlet and outlet moist air wet-bulb temperatures is needed. The bulk temperature of the product stream, T_p, can be found by first evaluating the bulk enthalpy of the condensate stream, h_b, and then using steam tables to look up the temperature as a function of enthalpy and pressure:

$$T_p = T\Big[h_b(T_{WB,in}, T_{WB,out}), p\Big] \tag{4}$$

The bulk temperature of the product stream can be found by evaluating the following integral, which assumes continuous removal of condensate from the condensing surface [21]:

$$\dot{H}_b = \dot{m}_a \int_{T_{WB,out}}^{T_{WB,in}} h_f(T_{WB}) \left(\frac{d\omega}{dT_{WB}}\right) dT_{WB} \tag{5}$$

The bulk enthalpy is converted to specific enthalpy by dividing through by the mass flow rate of product water:

$$h_b = \frac{\dot{H}_b}{\dot{m}_b} = \frac{\dot{H}_b}{\dot{m}_a(\omega_{in} - \omega_{out})} \tag{6}$$

where ω is the humidity ratio, defined as the ratio of mass of water vapor to mass of dry air. Finally, in order to reduce computational time, Eqs. (4)–(6) are solved before the simulation and the results are fitted to a polynomial function by using a least-squares surface fit. The fit is performed in MATLAB [22] using property data from REFPROP.

For the case of atmospheric pressure, the condensate temperature, as a function of inlet and outlet wet-bulb temperatures is given by

$$\begin{aligned} T_p(T_{WB,in}, T_{WB,out}) = {} & 0.0051918 T_{WB,in}^2 + 0.0027692 T_{WB,out}^2 \\ & -0.007417 T_{WB,in} T_{WB,out} \\ & -0.41913 T_{WB,in} + 1.0511 T_{WB,out} \\ & +61.6186 \end{aligned} \tag{7}$$

where all of the temperatures are in kelvin. Equation (7) is valid for $293\,\mathrm{K} \leq T_{WB} \leq 363\,\mathrm{K}$ and has a maximum relative error of less than 0.5% and a maximum absolute error of less than 1.4 K. Note that when the air stream is saturated, the wet-bulb temperature is equal to the dry bulb temperature.

3.4.2. Air and Water Heaters

The air and water heaters are single-stream heat exchangers in which composition of the stream remains constant. The First and Second Laws for a single-stream heat exchanger control volume reduce to:

$$\dot{Q}_{HT} = \dot{m}_h \left(h_{HT,out} - h_{HT,in} \right) \tag{8}$$

$$\dot{S}_{gen,HT} = \dot{m}_h \left(s_{HT,out} - s_{HT,in} \right) - \dot{S}_{trans,HT} \tag{9}$$

where m_h is the mass flow rate of the stream that is being heated in the heater. Heat transfer from the surroundings, $\dot{Q}_{HT}$, results in a corresponding entropy transfer to the working fluid, $\dot{S}_{trans,HT}$.

The entropy transfer is calculated assuming that the stream is heated with a constant heat flux per unit length, $\dot{Q}_{HT}/L$ [W/m], and that the wall temperature is greater than that of the bulk stream by a constant ΔT. Based on known results for solar collectors

[23], both approximations are reasonable. Since the temperature range is not large (less than 50 K), the heated stream's specific heat capacity is evaluated as constant at the average stream temperature and the bulk fluid temperature as a function of the axial coordinate, x, is given by

$$T_b(x) = T_{HT,in} + \frac{\left(\dot{Q}_{HT}/L\right)}{\dot{m}_h c_{p,h}} x \tag{10}$$

The wall temperature is:

$$T_{wall}(x) = T_b(x) + \Delta T = (T_{HT,in} + \Delta T) + \frac{\left(\dot{Q}_{HT}/L\right)}{\dot{m}_h c_{p,h}} x \tag{11}$$

The rate of entropy transfer can then be calculated as follows [24, 25]:

$$\begin{aligned} \dot{S}_{trans,HT} &= \int_0^L \frac{\dot{Q}_{HT}(x)}{T_{wall}(x)}\, dx \\ &= \dot{m}_h c_{p,h} \log\left[\frac{\dot{Q}_{HT}}{\dot{m}_h c_{p,h}\left(T_{HT,in} + \Delta T\right)} + 1\right] \end{aligned} \tag{12}$$

Once the entropy transfer is determined, calculation of the entropy generation within the fluid control volume is performed using the Second Law, Eq. (9).

3.5. HD Cycles

As discussed in Sec. 2, HD cycles can be formed by piecing together humidifiers, dehumidifiers, and heaters in the appropriate configuration. Since the dehumidifiers and humidifiers must come in pairs, as seen in Figs. 1 and 2, it is convenient to perform mass balances on both components simultaneously. The mass balances on the air and

water streams give the following relations:

$$\dot{m}_p = \dot{m}_a \left(\omega_{D,a,in} - \omega_{D,a,out}\right) \tag{13}$$

$$\dot{m}_b = \dot{m}_{w,H} - \dot{m}_a \left(\omega_{H,a,out} - \omega_{H,a,in}\right) = \dot{m}_{w,H} - \dot{m}_p \tag{14}$$

where $\dot{m}_a$ is the flow rate of dry air in the moist air stream, $\dot{m}_b$ is the flow rate of the brine stream, $\dot{m}_p$ is the flow rate of the condensate stream, $\dot{m}_{w,H}$ is the flow rate of water entering the humidifier, and ω is the humidity ratio on a mass basis. Note that the mass flow rate of seawater through the dehumidifier, $\dot{m}_w$, is constant. For convenience, the ratio of the seawater flow rate in the dehumidifier to the flow rate of dry air is defined as:

$$m_r \equiv \frac{\dot{m}_{w,D}}{\dot{m}_a} \tag{15}$$

The equations for each of the components, coupled with the mass balances, as well as proper matching of inlet and outlet streams from one component to the next forms a well-posed set of equations for the HD cycles.

3.6. Performance Parameters

There are several ways to characterize the performance of HD systems. Some important parameters are defined below.

3.6.1. Gained Output Ratio

The gained output ratio (GOR), sometimes known as the performance ratio, is a dimensionless measure of the amount of product produced for a given heat input. Here, it is defined as:

$$\mathrm{GOR} \equiv \frac{\dot{m}_p h_{fg}}{\dot{Q}_{in}} \tag{16}$$

where h_{fg} is the heat of vaporization evaluated at the inlet water temperature. For the cycles considered here, $\dot{Q}_{in} = \dot{Q}_{HT}$.

A GOR of 1 means that the system requires enough heat input to directly vaporize all of the produced water and that there is ineffective energy recovery. A basic solar still will have a GOR of approximately 1, or less owing to losses. A high GOR is desirable since it means that less heat input is required per unit water produced. When the heat source is a fossil fuel, higher GOR means lower fuel costs. When the heat source is solar radiation, higher GOR means a smaller solar collector area and hence, reduced capital costs.

3.6.2. Specific Entropy Generation

Specific entropy generation for the cycle is defined as the total entropy generated in all of the components within the desalination system divided by the mass flow rate of product water.

$$s_{gen,total} = \frac{\dot{S}_{gen,total}}{\dot{m}_p} \tag{17}$$

Thermodynamic arguments for the use of this parameter in analysis of HD cycles, based on the least heat of separation, are provided by Mistry et al. [5].

3.7. Simulations

Modeling in JACOBIAN was done in a modular fashion. First, models of the dehumidifier, humidifier, and heaters were constructed. Next, models of the various CAOW and OAOW cycles were created by including the components, connecting the appropriate streams and performing mass balances on each humidifier/dehumidifier pair.

After the cycle models were created, a separate block for each simulation was required. Simulations instantiate one or multiple models and fix the degrees of freedom. The advantage of this approach is that a single model (either for a component, or a cycle as a whole) can be used in multiple simulations. Therefore, simple variations of

each of the models, including operating conditions and configurations, can be analyzed without having to duplicate code.

4. Optimization Methods

The general form of the optimization problems solved is

$$\begin{aligned} &\min_{\mathbf{x}} f(\mathbf{x}) \\ &\text{such that } \mathbf{g}(\mathbf{x}) \leq \mathbf{0} \\ &\qquad \mathbf{x} \in [\mathbf{x}^L, \mathbf{x}^U], \qquad \mathbf{x}^L, \mathbf{x}^U \in \mathbb{R}^n \end{aligned}$$

where $\mathbf{x}$ are termed the optimization variables, $\mathbf{x}^L$ and $\mathbf{x}^U$ are the variable bounds, $f : [\mathbf{x}^L, \mathbf{x}^U] \to \mathbb{R}$ is the objective function and $\mathbf{g} : [\mathbf{x}^L, \mathbf{x}^U] \to \mathbb{R}^m$ are the inequality constraints.

The optimization problem at hand was solved using the so-called sequential mode of optimization in which the optimization problem is separated from the simulation. Only the degrees of freedom were used as optimization variables, resulting in small-scale optimization problems with relatively expensive function and gradient evaluations.

The optimization algorithm selects values for these optimization variables and then calls the simulator (JACOBIAN) to evaluate the objective function and constraints. The simulator sees these optimization variables as parameters in the model equations. For gradient-based methods, the gradients of these functions with respect to the optimization variables must be evaluated at each major iteration. In general, the model in JACOBIAN is represented by a system of differential-algebraic equations along with initial conditions, and the system is integrated in time. JACOBIAN then returns these gradients via an efficient calculation of the parametric sensitivities [26]. For the steady-state problem currently being considered, JACOBIAN has to solve a system of algebraic

equations only.

In order to optimize the system for maximum GOR, the main optimization variables considered are the mass flow rates, temperatures, and component effectivenesses. The simulator has to solve the model equations and calculate the cycle performance as a function of these variables. The problem constraints which the optimizer must satisfy are positive entropy generation and minimum terminal temperature difference. The optimization problems solved have 4 optimization variables with 8 constraints, and the embedded simulation problems include approximately 700 state variables, depending on the particular cycle being considered.

Two different gradient-based optimization solvers were used in this study, SNOPT and IPOPT. SNOPT [6, 7] is based on a sparse successive quadratic programming algorithm with limited-memory quasi-Newton approximations to the Hessian of the Lagrangian. SNOPT is a commercial code distributed as a set of Fortran 77 subroutines which can be also converted to C code. IPOPT [8] is an interior point method intended for large-scale optimization problems implemented in C++. IPOPT is released as open source code under the Common Public License (CPL), and can be linked from various languages including C/C++, C, Fortran, AMPL and MATLAB on various computer platforms. IPOPT can use first- and second-order derivatives of the objective function and constraints with respect to the optimization variables. Herein, only first derivatives are returned by JACOBIAN and IPOPT uses an approximation for the Hessian. Default values are used for the options and tolerances in JACOBIAN. For the optimization, the tolerances are set to 10^{-4}. Each local optimization run takes on the order of 10–30 seconds when performed on a server consisting of PCs with two Intel Xeon E5405 quad core CPUs at 2.00 GHz (eight cores total) with 8 GB of RAM.

The gradient-based optimizers used generate local optima. Unfortunately, due to the nonconvexity of the modeling equations, local optimality does not imply global

optimality. In fact, for the case studies presented, the solution depends on the initial guess provided for each of the optimization variables. To overcome this limitation of the solvers, a multi-start heuristic was used. The initial guess is initialized randomly and 1000 optimization runs were executed in a computer cluster. As a consequence, the solutions reported cannot be rigorously guaranteed to be optimal. However, both solvers with multiple initial guesses converged to the same solution, thus giving high confidence that this is a global solution. Additionally, a genetic algorithm running for over 50 hours did not yield a better solution. Moreover, an in-house translation script was used to convert the JACOBIAN models to the optimization modelling environment, GAMS [27], in order to enable the use of additional solvers. Through GAMS, the solvers CONOPT [28, 29], KNITRO [30], and MINOS [31] were also used in order to further verify the results. In future work, deterministic global optimization will also be employed, in particular the branch and reduce code BARON [32, 33].

5. Results

5.1. Closed Air, Open Water (CAOW) Cycles

The choice of bounds for the optimization variables is governed based on the findings from earlier studies of these cycles [4, 5]. A summary of the variable bounds and constraints is presented in Table 1. Based on heuristic search efforts in [5], the optimal GOR for the water heated cycles was always in the range of mass flow rate ratios of approximately $1 < m_r < 4$ while for the air heated cycles, peak GOR was typically between $0.5 < m_r < 1.5$. Here, the overall mass flow rate ratio range is extended to $0.4 < m_r < 6$ in order to ensure that the optimal conditions would be within the variable bounds. Similarly, it was previously seen that peak performance quickly dropped off with decreasing component effectiveness, as expected. Therefore, effectiveness is bounded to $0.8 \leq \epsilon_D, \epsilon_H \leq 1.0$. By selecting a minimum effectiveness of 80% rather

than the physical minimum of 0%, the variable domain space is greatly reduced, which is particularly important for the multistart procedure, but is also expected to help the local searches.

Finally, two different top temperature conditions are considered. First, the overall system top temperature (the temperature of the fluid exiting the heater) is limited to $323.15\,\mathrm{K} \leq T_{top} \leq 370.15\,\mathrm{K}$. The lower limit is selected based on the results from previous studies. The upper limit is selected as a representative limit for scale formation. Scaling is caused by several factors related to the concentration of certain solutes, especially $CaSO_4$, exceeding their solubility limit (supersaturation). Accordingly, thermal desalination processes are normally limited to temperatures below the normal boiling point [34]. While scale formation is still an issue at elevated temperatures, maintaining the fluid below the boiling point prevents further concentration of salts through boiling and evaporation. Also, the solubility limit of calcium sulfate, one of the primary components in seawater scaling, decreases with increasing temperature. Therefore, maintaining a lower seawater temperature helps to reduce the degree of supersaturation of $CaSO_4$. Initial optimization results showed that the best WH cycles operate with a maximum seawater temperature below 353.15 K while the AH cycles operate at a higher maximum moist air temperature, but lower maximum seawater temperature. In order to enforce even more conservative conditions on the systems, a second round of optimization is performed in which the maximum seawater temperature, $T_{H,w,in}$, is constrained to be less than 343.15 K since existing multieffect distillation desalination systems typically do not exceed this water temperature [35].

[Table 1 about here.]

Constraints are selected in order to ensure that the Second Law of Thermodynamics is not violated and that the components are of reasonable size. First, the entropy

generation within each component is constrained to be greater than zero. Second, the terminal temperature difference (TTD), or approach temperature, is selected to be no smaller than typical values found in existing equipment. The Standard Handbook of Plant Engineering has charts that show the approach of cooling towers to be as small as 2 °F (1.11 K) [36]. Such small TTDs require very large surface areas as seen by the plot of tower size factor versus terminal temperature difference in Fig. 6, which has been redrawn from Cooling Tower Fundamentals [37]. In order to ensure that the hardware size is reasonable, a parametric study was performed with TTD from 2–6 K. Based on Fig. 6, a TTD of 6 K has a tower size factor of approximately 1.4 while a TTD of 3 K has a size factor of approximately 2.2. Note that a control volume analysis coupled with these constraints provides a necessary set of conditions to ensure that the Second Law is not violated. However, it is not sufficient to guarantee the absense of internal temperature cross. The TTD constraints were selected based on the operating conditions of real equipment since temperature cross does not occur in real hardware.

[Figure 6 about here.]

In addition to the variable bounds and constraints, input conditions must be specified. For all of the calculations, all components are assumed to operate at atmospheric pressure and the feedwater inlet temperature is assumed to be 303.15 K based on typical temperatures for the Red Sea [38]. For the open air cycles, the ambient conditions are selected to be

$$\begin{aligned} p_0 &= 101.325\,\text{kPa} \\ T_0 &= 303.15\,\text{K} \end{aligned} \tag{18}$$

Using the specified variable bounds and system constraints, the SNOPT and IPOPT local solvers are used with the multi-start code in order to find a global maximum GOR for both the CAOW-WH and CAOW-AH cycles. The optimized results for the CAOW-WH cycle are presented in Table 2 while results for the CAOW-AH cycle are presented

in Table 3. The previous best case configurations that were found without the aid of optimization, using heuristic methods and by varying parameters one at a time, are also included in these two tables for comparison. The results from both cycle configurations are plotted in Fig. 7.

[Table 2 about here.]

For the CAOW-WH cycle, GOR is improved 60% (from 2.53 to 4.04) when considering the case with a minimum approach of 3 K. In each case, it is clear that the largest changes in operating conditions were in the mass flow rate ratio and the effectiveness of the dehumidifier while the system top temperature and humidifier effectiveness vary only slightly. GOR for these cycles is quite sensitive to both flow rates and component effectivenesses. The sensitivity to the mass flow rate ratio shows that these systems require accurate control over the flow rates of the two streams in order to maintain optimal conditions. The sensitivity to effectiveness shows that it is essential to use properly designed components in order to achieve peak performance. As the effectivenesses of the components increases, both the size and cost of the cycle increase. Note that effectiveness does not reach 100% since doing so would violate either the TTD or the entropy generation constraint. Also note that the specific entropy generation for the cycle decreased significantly at optimized conditions as expected since minimizing specific entropy generation results in maximum GOR [5].

[Table 3 about here.]

Similar behavior is seen in the CAOW-AH cycle. A 51% improvement in GOR (from 3.48 to 5.27), for a minimum TTD of 3 K, is achieved by making a large change to the mass flow rate ratio and smaller changes to the component effectiveness and top temperature. Again, the specific entropy generation decreased and the recovery ratio increased.

[Figure 7 about here.]

In Fig. 7, two trends are apparent. First, as the terminal temperature difference increases, the performance of the cycles drops. This is an expected trend since a larger TTD results in increased entropy generation due to larger temperature gradients. Additionally, larger TTDs imply lower regeneration in either the humidifier or the dehumidifier as a result of the large temperature difference of the outlet streams.

The second trend is that the air heated cycle is much more sensitive to TTD than is the water heated cycle. This can be explained by considering the energy regeneration of each cycle. In the WH cycle, hot seawater is used in the humidifier to transfer both moisture and energy to the cooler air stream. Since the water stream enters the humidifier at an elevated temperature, the air stream gains a large amount of moisture prior to entering the dehumidifier. In the AH cycle, hot air enters the dehumidifier and heats up the seawater stream. The warm seawater stream then enters the dehumidifier and humidifies the cooler air stream. When the TTD in the dehumidifier increases, the energy regeneration in the dehumidifier decreases significantly, resulting in a lower seawater top temperature. The lower seawater temperature results in lower potential for driving the humidification process and the air stream picks up less moisture in the humidifier. Less moisture content in the air ultimately means that less water is produced and the cycle performance decreases. When the TTD in the AH cycle is low, however, energy regeneration in the AH cycle is more efficient than that in the WH cycle.

A second, more conservative, round of optimization is performed by imposing the constraint on maximum water temperature. The results for both the CAOW-WH cycle and the CAOW-AH cycle are presented in Tables 4 and 5 respectively. Additionally, GOR is plotted versus TTD for both cases in Fig. 8.

[Table 4 about here.]

[Table 5 about here.]

Figure 8 shows that the same general trends are present even when the maximum water temperature constraint is imposed. However, a major difference between Fig. 7 and Fig. 8 is that as the TTD increases, the performance of both the CAOW-AH and CAOW-WH cycles converge to values that are lower than either performance values found in Fig. 7. When the system is limited by the seawater top temperature constraint, effectively, the system top temperature is also limited. This lowering of the maximum operating temperature results in the observed reduction in performance.

[Figure 8 about here.]

Since the cost and size of the dehumidifier and humidifier increases with decreasing TTD, it is clear that an inexpensive HD system for developing regions (which would have less efficient components) should be water heated since the WH cycles outperform the AH cycles as TTD increases (or performs similarly when the maximum water temperature is limited). In addition, solar water heaters tend to be cheaper and more readily available than air heaters [3, 39].

5.2. Open Air, Open Water (OAOW) Cycles

For open air cycles, the ambient air conditions introduce two additional parameters to be considered: inlet air temperature and inlet air relative humidity. The air temperature is taken to be equal to the ambient air temperature of 303.15 K specified in the CAOW section. The inlet relative humidity, $\phi_{H,a,in}$, is treated as a variable since the performance of the OAOW cycles is strongly dependent on the inlet humidity. The other variable bounds and constraints for the OAOW cycles are unchanged from the CAOW (Table 1).

5.2.1. OAOW-WH Cycles

Figure 9 shows a plot of the optimized GOR values for a OAOW-WH cycle with a minimum TTD of 4 K versus the air inlet relative humidity. The TTD is selected to be 4 K since this TTD offers a reasonable compromise between component size and effectiveness. Note that each point represents an optimized value of the best performance achievable (result of parametric optimization) with different component effectivenesses, top temperature, and mass flow rate ratio. Additionally, GOR for a CAOW-WH cycle with a minimum TTD of 4 K is also plotted on the figure for reference (constant since the CAOW cycles are not affected by ambient air conditions).

[Figure 9 about here.]

Figure 9 clearly shows that the OAOW-WH cycle outperforms the CAOW-WH cycle, regardless of the ambient relative humidity. Additionally, the performance of the cycle improves as the relative humidity decreases. This result may seem counterintuitive since the open cycle exhausts warm saturated air from the dehumidifier to the environment.

The primary factor that contributes to the improved performance of the OAOW-WH cycle is that cooler air entering the humidifier (even when saturated) has a lower moisture content than the saturated, warmer air found in the CAOW cycle. Therefore, it has greater potential to absorb moisture from the warm seawater stream.

This unexpectedly good performance of OAOW cycles was found through the optimization efforts. Initial calculations on the OAOW-WH cycles resulted in inferior GOR values than were achieved using the CAOW-WH cycles. However, after applying optimization, the potential of the OAOW-WH cycles was revealed.

5.2.2. OAOW-AH Cycles

Figure 10 shows a plot of the optimized GOR values for a OAOW-AH cycle with a minimum TTD of 4 K versus the air inlet relative humidity. As before, each point represents an optimized value of the best performance achievable with different component effectivenesses, top temperature, and mass flow rate ratio. For comparison, GOR for a CAOW-AH cycle with a minimum TTD of 4 K is also plotted on the figure.

[Figure 10 about here.]

Unlike the water heated case, Fig. 10 shows that the performance of the air heated cycle increases with increasing ambient relative humidity. Further, with the exception of very high ambient relative humidity, the CAOW-AH cycle outperforms the OAOW-AH cycle.

To explain the trend of decreasing GOR with decreasing ambient relative humidity, consider the humidification process. When unsaturated air enters the humidifier, it is simultaneously humidified and heated. However, as the inlet humidity decreases, the exit temperature of the air stream also decreases since the stream needs to first reach saturation before substantially increasing in temperature. Since drier inlet air results in a lower humidifier exit temperature, $T_{H,a,out}$, more heating is required to raise the moist air temperature to the system top temperature, $T_{\max} = T_{HT,out}$. As the required heating increases, the performance of the system rapidly drops since GOR is inversely related to the required heat input, as seen in Eq. (16). Additionally, the warm saturated air that exits the dehumidifier is exhausted to the environment. The temperature and moisture content of the exhaust stream from AH cycles is greater than the temperature and moisture content of the WH exhaust stream, resulting in further losses which lower the performance of the system.

Figure 10 shows that at very high ambient relative humidities, the performance of the open air cycle is greater than that of the closed air cycle. When the ambient

air is saturated, $\phi_{H,a,in} = 1$, the only difference between the CAOW-AH and OAOW-AH cycles is that $T_{H,a,in}$ equals the ambient temperature, T_0, instead of $T_{D,a,out}$. In general, the ambient temperature of the air will be less than the dehumidifier exhaust temperature. As a result, the humidifier in the OAOW-AH cycle is operating with a lower inlet temperature. The lower temperature air stream provides a greater potential for heat and mass transfer exchange with the warm seawater stream. Therefore, the humidifier can run at a higher effectiveness which leads to improved cycle performance.

Based on the results of optimizing the OAOW-AH cycles, it is clear that while the open air cycles outperform the closed air cycles for near saturated ambient conditions, the performance of the OAOW-AH quickly drops as the ambient relative humidity decreases. Therefore, in general, the CAOW-AH cycle will outperform the OAOW-AH cycles.

5.2.3. Comparison of OAOW Cycles

In order to see how the performance of the OAOW cycles varies with respect to minimum TTD, a parametric study is performed with TTD from 2–6 K, as is done with the CAOW cycles. The same variable bounds and constraints used for the CAOW are imposed on the OAOW cycles. The ambient relative humidity is selected to be $\phi_0 = 0.6$.

Using the specified variable bounds and system constraints with multi-start optimization, the global maximum GOR for both OAOW-WH and OAOW-AH cycles is determined. The optimized results for the OAOW-WH cycle are presented in Table 6 while results for the OAOW-AH cycle are presented in Table 7. The results from both cycle configurations are plotted in Fig. 11.

[Table 6 about here.]

[Table 7 about here.]

[Figure 11 about here.]

Figure 11 and Tables 6 and 7 show the same trends as what is seen in the CAOW results (Fig. 7, Table 2, and Table 3). That is, GOR drops significantly with increasing TTD, specific entropy generation is minimum for the optimized conditions, and the cycles are sensitive to both the mass flow rate ratio and component effectiveness. One observable difference between the OAOW cycles and the CAOW cycles is that unlike in the CAOW cycles, the optimized OAOW-WH cycle outperforms the optimized OAOW-AH cycle, regardless of specified TTD.

6. Conclusions

Multi-parameter optimization methods have been used to find the optimal operating conditions for both CAOW and OAOW humidification-dehumidification desalination cycles and to investigate some characteristics of the various cycles. The following conclusions were reached:

1. The use of systematic optimization methods for analysis of HD cycles found operating conditions having substantially improved performance compared to those found in previous studies. Some of these performance gains were achieved through selection of counterintuitive cycle configurations and operating conditions. The improved operating conditions occur when the humidifier and dehumidifier have higher effectiveness.
2. For a TTD of 3 K, the CAOW-WH cycle can achieve a GOR of 4.06 while the CAOW-AH cycle can achieve a GOR of 5.29.
3. As the TTD increases, the performance of both CAOW-WH and CAOW-AH cycles decreases. At low TTD, the air heated cycle outperforms the water heated cycle while at higher TTD, the water heated cycle outperforms the air heated

cycle. When the maximum water temperature is limited, the performance of the AH and WH cycles converge.

4. The optimized OAOW-WH cycle always outperforms the optimized CAOW-WH cycle, regardless of ambient relative humidity.
5. The optimized OAOW-AH cycle generally performs worse than the optimized CAOW-AH cycle except when ambient relative humidity is near 100%.

7. Acknowledgments

The authors would like to thank the King Fahd University of Petroleum and Minerals for funding the research reported in this paper through the Center for Clean Water and Clean Energy at MIT and KFUPM. The authors would also like to thank Numerica Technology for providing access to the JACOBIAN software for this research.

[1] S. Parekh, M. M. Farid, J. R. Selman, S. Al-hallaj, Solar desalination with a humidification-dehumidification technique — a comprehensive technical review, Desalination 160 (2004) 167–186.

[2] E. Chafik, Design of plants for solar desalination using the multi-stage heating/humidifying technique, Desalination 168 (2004) 55–71. Desalination Strategies in South Mediterranean Countries.

[3] G. P. Narayan, M. H. Sharqawy, E. K. Summers, J. H. Lienhard V, S. M. Zubair, M. Antar, The potential of solar-driven humidification-dehumidification desalination for small-scale decentralized water production, Renewable and Sustainable Energy Reviews 14 (2010) 1187–1201.

[4] G. P. Narayan, M. H. Sharqawy, J. H. Lienhard V, S. M. Zubair, Thermodynamic analysis of humidification dehumidification desalination cycles, Desalination and Water Treatment 16 (2010) 339–353.

[5] K. H. Mistry, J. H. Lienhard V, S. M. Zubair, Effect of entropy generation on the performance of humidification-dehumidification desalination cycles, International Journal of Thermal Sciences 49 (2010) 1837–1847.

[6] P. E. Gill, W. Murray, M. A. Saunders, SNOPT, 2006.

[7] P. E. Gill, W. Murray, M. A. Saunders, SNOPT: An SQP Algorithm for Large-Scale Constrained Optimization, SIAM Journal on Optimization 12 (2002) 979–1006.

[8] A. Wächter, L. T. Biegler, On the implementation of an interior-point filter line-search algorithm for large-scale nonlinear programming., Mathematical Programming 106 (2006) 25–57.

[9] S. A. Klein, Engineering Equation Solver, Academic Professional, Version 8, 2010.

[10] Numerica Technology, JACOBIAN Modeling and Optimization Software, http://www.numericatech.com, 2009.

[11] S. Eftekharzadeh, M. M. Baasiri, P. A. Lindahl Jr., Feasibility of Seawater Cooling Towers for Large-Scale Petrochemical Development, Technical Report TP03-17, Cooling Technology Institute, San Antonio, Texas, 2003.

[12] M. H. Sharqawy, J. H. Lienhard V, S. M. Zubair, Thermophysical properties of seawater: A review of existing correlations and data, Desalination and Water Treatment 16 (2010) 354–380.

[13] M. H. Sharqawy, J. H. Lienhard V, S. M. Zubair, On thermal performance of seawater cooling towers, in: Proceedings of the International Heat Transfer Conference IHTC14, 23200, 14$^{\text{th}}$ International Heat Transfer Conference, Washington, DC, USA. August 8–13, 2010.

[14] E. W. Lemmon, R. T. Jacobsen, S. G. Penoncello, D. G. Friend, Thermodynamic Properties of Air and Mixtures of Nitrogen, Argon, and Oxygen From 60 to 2000 K at Pressures to 2000 MPa, Journal of Physical and Chemical Reference Data 29 (2000) 331–385.

[15] E. W. Lemmon, M. L. Huber, M. O. McLinden, NIST Standard Reference Database 23: Reference Fluid Thermodynamic and Transport Properties-REFPROP, Version 8.0, 2007.

[16] J. R. Cooper, Revised Release on the IAPWS Industrial Formulation 1997 for the Thermodynamic Properties of Water and Steam, The International Association for the Properties of Water and Steam - (2007) 1–48.

[17] D. J. Wessel, ed., ASHRAE Fundamentals Handbook 2001 (SI Edition), American Society of Heating, Refrigerating, and Air-Conditioning Engineers, 2001.

[18] R. W. Hyland, A. Wexler, Formulations for the Thermodynamic Properties of the Saturated Phases of H2O from 173.15 K to 473.15 K, ASHRAE Transactions Part 2A (RP-216) (1983a) 500–519.

[19] G. P. Narayan, J. H. L. V, S. M. Zubair, Entropy generation minimization of combined heat and mass transfer devices, International Journal of Thermal Sciences 49 (2010) 2057–2066.

[20] G. P. Narayan, K. H. Mistry, M. H. Sharqawy, S. M. Zubair, J. H. Lienhard V, Energy effectiveness of simultaneous heat and mass exchange devices, Frontiers in Heat and Mass Transfer 1 (2010) 1–13.

[21] K. H. Mistry, Second Law Analysis and Optimization of Humidification-Dehumidification Desalination Cycles, Master's thesis, Massachusetts Institute of Technology, Cambridge, MA, 2010.

[22] The MathWorks, MATLAB R2008A, 2008.

[23] J. A. Duffie, W. A. Beckman, Solar Engineering of Thermal Processes, John Wiley & Sons, Inc., Hoboken, New Jersey, 3rd edition, 2006.

[24] A. Bejan, Advanced Engineering Thermodynamics, John Wiley & Sons, Inc., Hoboken, New Jersey, 3rd edition, 2006.

[25] M. J. Moran, H. N. Shapiro, Fundamentals of Engineering Thermodynamics, John Wiley & Sons, Inc., New Jersey, 6th edition, 2007.

[26] W. F. Feehery, J. E. Tolsma, P. I. Barton, Efficient sensitivity analysis of large-scale differential-algebraic systems, Applied Numerical Mathematics 25 (1997) 41–54.

[27] A. Brooke, D. Kendrick, A. Meeraus, GAMS: A User's Guide, The Scientific Press, Redwood City, California, 1988.

[28] A. S. Drud, CONOPT: A GRG code for large sparse dynamic nonlinear optimization problems, Mathematical Programming 31 (1985) 153–191.

[29] A. S. Drud, CONOPT–A Large-Scale GRG Code, INFORMS JOURNAL ON COMPUTING 6 (1994) 207–216.

[30] R. H. Byrd, J. Nocedal, R. A. Waltz, Large-Scale Nonlinear Optimization, volume 83, Springer, US, pp. 35–59.

[31] B. A. Murtagh, M. A. Saunders, MINOS 5.5 User's Guide, Report SOL 83-20R, Technical Report, Department of Operations Research, Stanford University, 1987.

[32] M. Tawarmalani, N. V. Sahinidis, A polyhedral branch-and-cut approach to global optimization, Mathematical Programming 103 (2005) 225–249.

[33] N. V. Sahinidis, BARON: A general purpose global optimization software package, Journal of Global Optimization 8 (1996) 201–205.

[34] K. S. Spiegler, Y. M. El-Sayed, A Desalination Primer: Introductory book for students and newcomers to desalination, Balaban Desalination Publications, Santa Maria Imbaro, Italy, 1994.

[35] L. Awerbuch, "Integrated Hybrid Desalination Systems Integrated Hybrid Desalination Systems" integration of desalination, power, integration of desalination, power, environment and security environment and security, in: International Conference on Non-Electric Applications of Nuclear Power: Seawater Desalination, Hydrogen Production and other Industrial Applications, International Atomic Energy Agency. 16–19 April 2007.

[36] R. C. Rosaler, Standard Handbook of Plant Engineering, McGraw-Hill, New York, NY, 3rd. edition, 2002.

[37] J. C. Hensley (Ed.), Cooling Tower Fundamentals, SPX Cooling Technologies, Inc., Overland Park, Kansas USA, 2nd edition, 2009.

[38] NOAA/OAR/ESRL PSD, International Comprehensive Ocean-Atmosphere Data Set (ICOADS), `http://www.esrl.noaa.gov/psd/data/gridded/data.coads.ltm.html`, Accessed 2010.

[39] E. K. Summers, J. H. Lienhard V, S. M. Zubair, Air-heating solar collectors for humidification-dehumidification desalination systems, in: Proceedings of the International Heat Transfer Conference IHTC14, 23214, International Heat Transfer Conference, Washington DC, USA. August 8–13, 2010.

List of Figures

1 A schematic diagram of a closed air, open water, water heated (CAOW-WH) cycle. 36
2 A schematic diagram of a closed air, open water, air heated (CAOW-AH) cycle. 37
3 A schematic diagram of an open air, open water, water heated (OAOW-WH) cycle. 38
4 A schematic diagram of an open air, open water, air heated (OAOW-AH) cycle. 39
5 Humidifier and dehumidifier control volumes. 40
6 Impact of terminal temperature difference on tower size using fresh water. Redrawn from CTI [37]. 41
7 GOR versus TTD for CAOW-WH and CAOW-AH cycles. 42
8 GOR versus TTD for CAOW-WH and CAOW-AH cycles with maximum water temperature constrained to less than 343.15 K. 43
9 GOR versus ambient relative humidity for OAOW-WH cycle with a minimum TTD of 4 K. GOR for CAOW-WH cycle also plotted for reference. 44
10 GOR versus ambient relative humidity for OAOW-AH cycle with a minimum TTD of 4 K. GOR for CAOW-AH cycle also plotted for reference. 45
11 GOR versus TTD for OAOW-WH and OAOW-AH cycles. 46

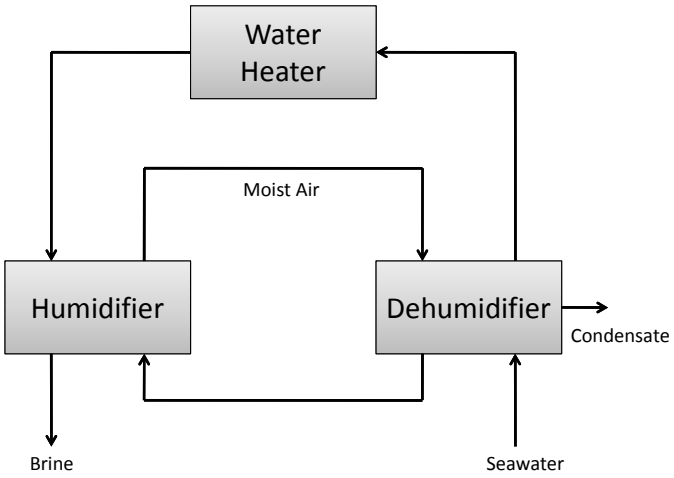

Figure 1: A schematic diagram of a closed air, open water, water heated (CAOW-WH) cycle.

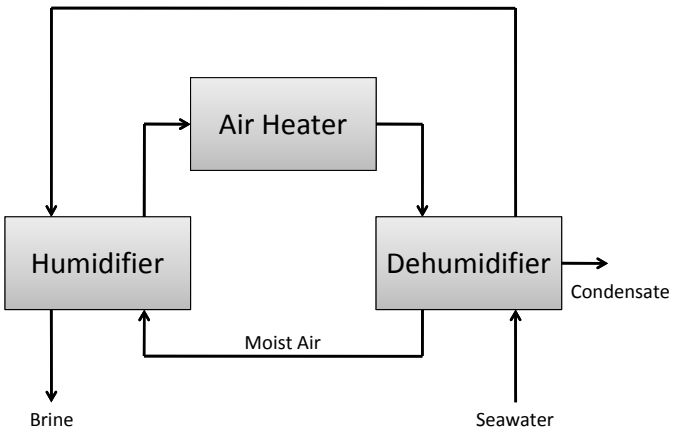

Figure 2: A schematic diagram of a closed air, open water, air heated (CAOW-AH) cycle.

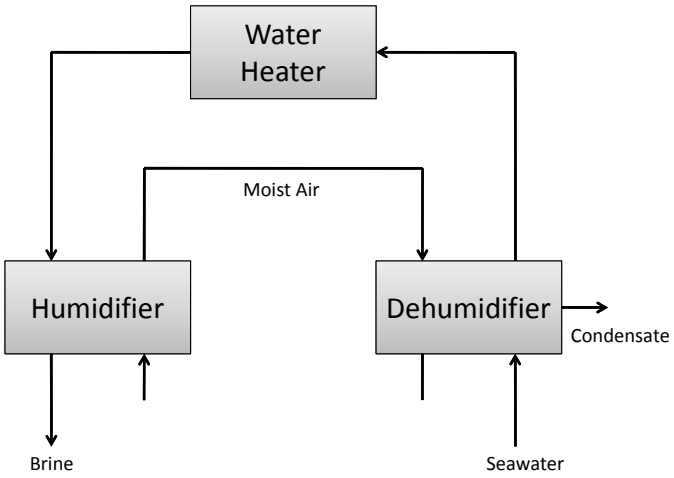

Figure 3: A schematic diagram of an open air, open water, water heated (OAOW-WH) cycle.

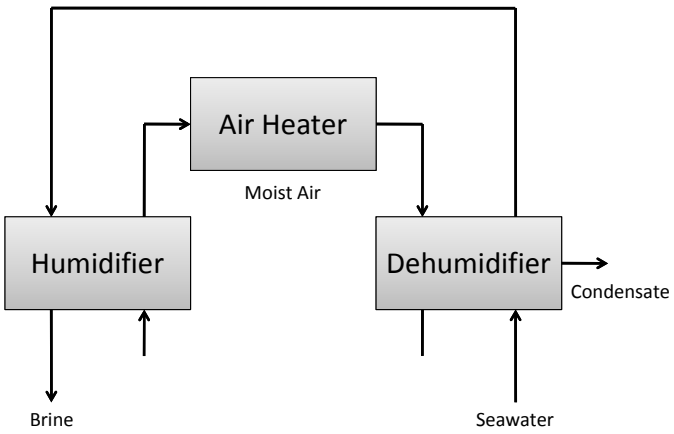

Figure 4: A schematic diagram of an open air, open water, air heated (OAOW-AH) cycle.

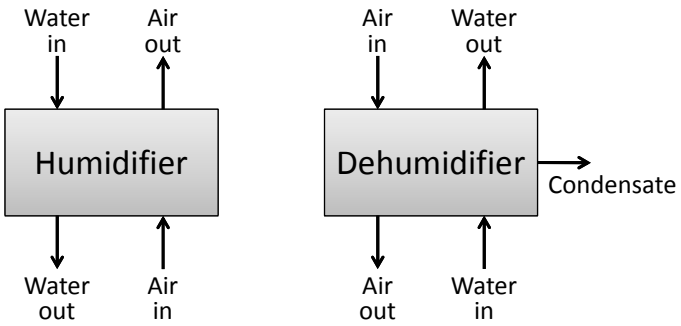

Figure 5: Humidifier and dehumidifier control volumes.

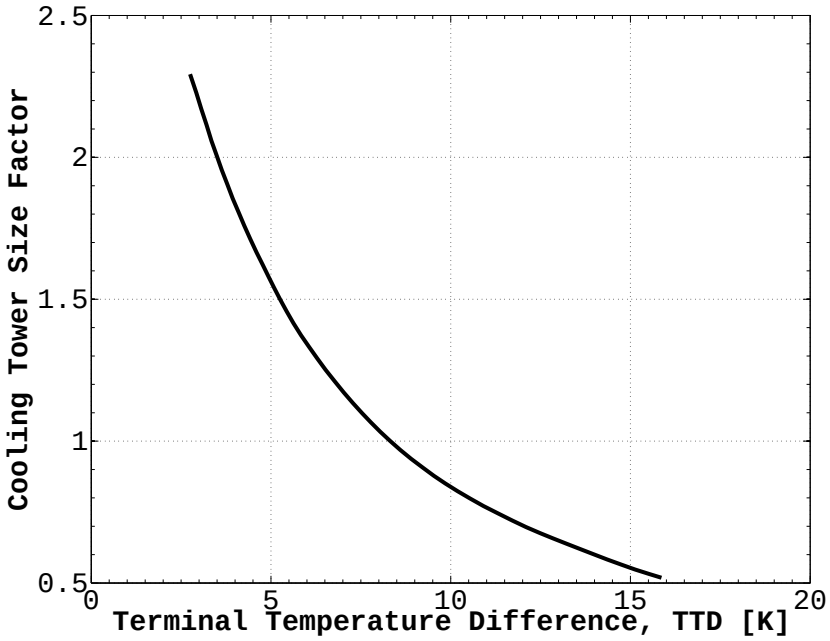

Figure 6: Impact of terminal temperature difference on tower size using fresh water. Redrawn from CTI [37].

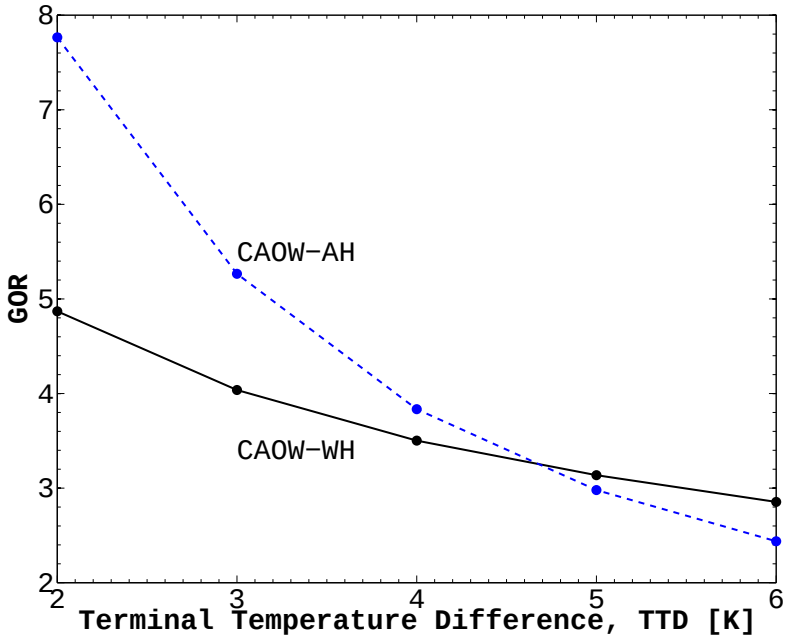

Figure 7: GOR versus TTD for CAOW-WH and CAOW-AH cycles.

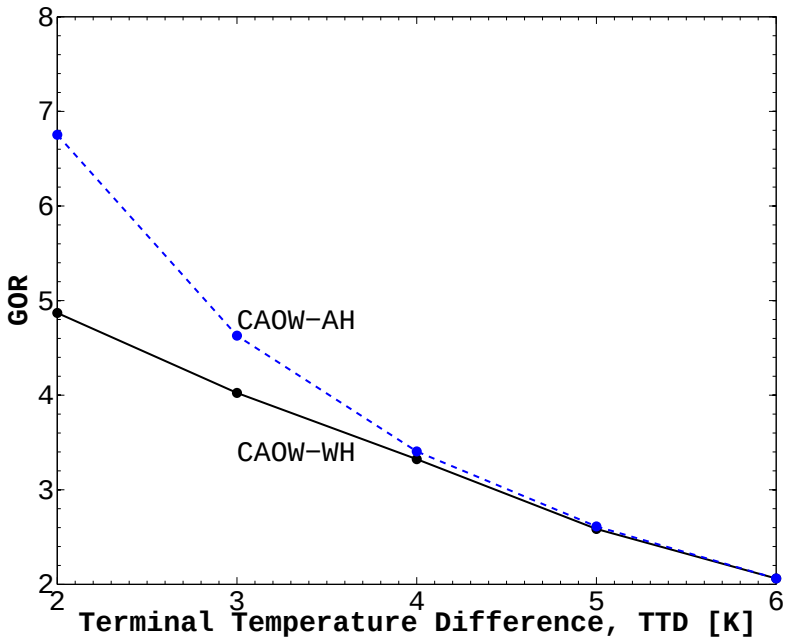

Figure 8: GOR versus TTD for CAOW-WH and CAOW-AH cycles with maximum water temperature constrained to less than 343.15 K.

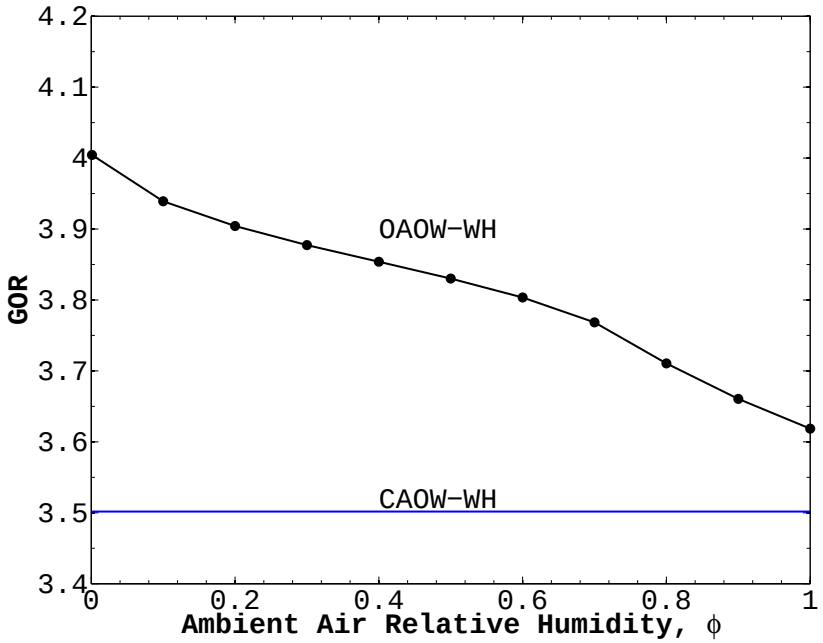

Figure 9: GOR versus ambient relative humidity for OAOW-WH cycle with a minimum TTD of 4 K. GOR for CAOW-WH cycle also plotted for reference.

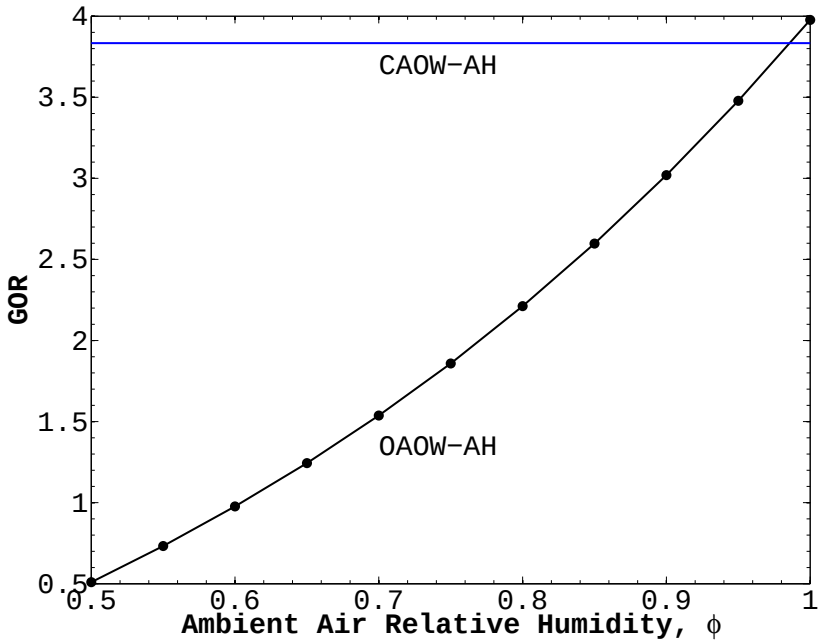

Figure 10: GOR versus ambient relative humidity for OAOW-AH cycle with a minimum TTD of 4 K. GOR for CAOW-AH cycle also plotted for reference.

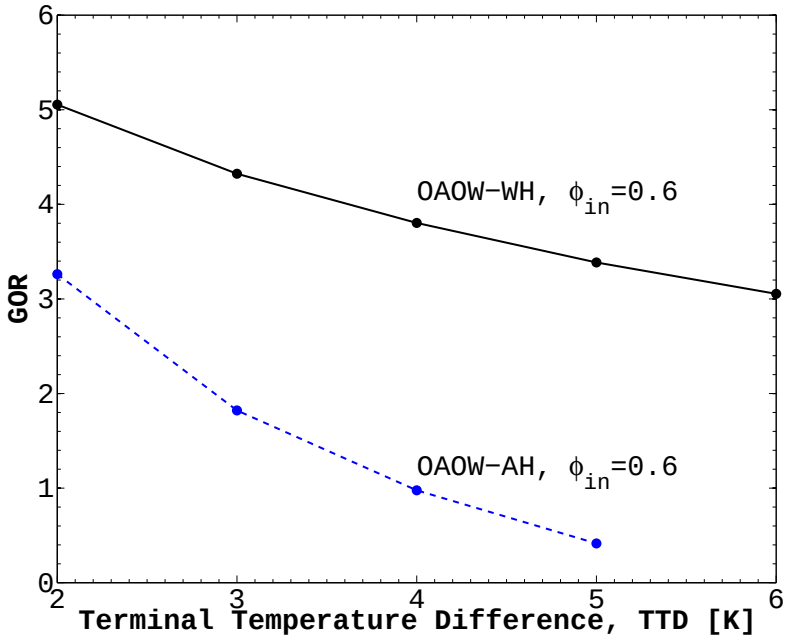

Figure 11: GOR versus TTD for OAOW-WH and OAOW-AH cycles.

List of Tables

1 Variable bounds and constraints used for optimization of CAOW and OAOW cycles. 48
2 CAOW-WH optimization results as a function of the minimum terminal temperature difference in either the humidifier or the dehumidifier. . . . 49
3 CAOW-AH optimization results as a function of the minimum terminal temperature difference in either the humidifier or the dehumidifier. . . . 50
4 CAOW-WH optimization results as a function of the minimum terminal temperature difference in either the humidifier or the dehumidifier with maximum water temperature constrained to less than 343.15 K. 51
5 CAOW-AH optimization results as a function of the minimum terminal temperature difference in either the humidifier or the dehumidifier with maximum water temperature constrained to less than 343.15 K. 52
6 OAOW-WH optimization results as a function of the minimum terminal temperature difference in either the humidifier or the dehumidifier, $\phi_{in} = 0.6$. 53
7 OAOW-AH optimization results as a function of the minimum terminal temperature difference in either the humidifier or the dehumidifier, $\phi_{in} = 0.6$. 54

Table 1: Variable bounds and constraints used for optimization of CAOW and OAOW cycles.

Variable Bounds	Low	High
m_r	0.4	6
ϵ_D, ϵ_H	0.8	1
T_{max}	333.15 K	370.15 K

Constraints	
$\dot{S}_{gen}$	≥ 0
TTD_D, TTD_H	$\geq$ 2–6 K
$T_{H,w,in}$	$\leq$ 343.15 K

Table 2: CAOW-WH optimization results as a function of the minimum terminal temperature difference in either the humidifier or the dehumidifier.

	Minimum Terminal Temperature Difference					
Parameter	Original (3.4 K)	2 K	3 K	4 K	5 K	6 K
GOR	2.53	4.87	4.04	3.50	3.14	2.85
s_{gen} [kW/K]	0.32	0.15	0.20	0.25	0.30	0.35
m_r	2.90	2.44	3.01	3.67	4.42	5.29
ϵ_D	0.90	0.96	0.96	0.96	0.96	0.96
ϵ_H	0.90	0.93	0.91	0.90	0.89	0.88
T_{min} [K]	303.15	303.15	303.15	303.15	303.15	303.15
T_{max} [K]	343.15	331.75	339.07	345.28	350.77	355.65

Table 3: CAOW-AH optimization results as a function of the minimum terminal temperature difference in either the humidifier or the dehumidifier.

	Minimum Terminal Temperature Difference					
Parameter	Original (3.4 K)	2 K	3 K	4 K	5 K	6 K
GOR	3.48	7.76	5.27	3.83	2.98	2.44
s_{gen} [kW/K]	0.28	0.15	0.21	0.28	0.35	0.41
m_r	1.22	2.12	1.74	1.46	1.24	1.07
ϵ_D	0.90	0.98	0.95	0.93	0.89	0.85
ϵ_H	0.90	0.96	0.93	0.91	0.88	0.85
T_{min} [K]	303.15	303.15	303.15	303.15	303.15	303.15
T_{max} [K]	363.15	370.15	370.15	370.15	370.15	370.15

Table 4: CAOW-WH optimization results as a function of the minimum terminal temperature difference in either the humidifier or the dehumidifier with maximum water temperature constrained to less than 343.15 K.

	Minimum Terminal Temperature Difference					
Parameter	Original (3.4 K)	2 K	3 K	4 K	5 K	6 K
GOR	2.53	4.87	4.02	3.32	2.59	2.06
s_{gen} [kW/K]	0.32	0.15	0.20	0.26	0.32	0.38
$T_{H,w,in}$ K	343.15	331.75	339.06	343.15	343.15	343.15
m_r	2.90	2.44	3.01	3.41	3.37	3.34
ϵ_D	0.90	0.96	0.96	0.95	0.94	0.92
ϵ_H	0.90	0.93	0.91	0.89	0.86	0.83
T_{min} [K]	303.15	303.15	303.15	303.15	303.15	303.15
T_{max} [K]	343.15	331.75	339.06	343.15	343.15	343.15

Table 5: CAOW-AH optimization results as a function of the minimum terminal temperature difference in either the humidifier or the dehumidifier with maximum water temperature constrained to less than 343.15 K.

	Minimum Terminal Temperature Difference					
Parameter	Original (3.4 K)	2 K	3 K	4 K	5 K	6 K
GOR	3.48	6.75	4.63	3.41	2.61	2.06
s_{gen} [kW/K]	0.28	0.15	0.22	0.29	0.36	0.49
$T_{H,w,in}$ K	337.40	343.15	343.15	343.15	343.15	343.15
m_r	1.22	1.78	1.54	1.30	1.10	1.15
ϵ_D	0.90	0.97	0.94	0.91	0.87	0.85
ϵ_H	0.90	0.95	0.92	0.89	0.86	0.83
T_{min} [K]	303.15	303.15	303.15	303.15	303.15	303.15
T_{max} [K]	363.15	358.20	361.99	363.22	362.70	372.87

Table 6: OAOW-WH optimization results as a function of the minimum terminal temperature difference in either the humidifier or the dehumidifier, $\phi_{in} = 0.6$.

	Minimum Terminal Temperature Difference				
Parameter	2 K	3 K	4 K	5 K	6 K
GOR	5.05	4.32	3.80	3.39	3.05
s_{gen} [kW/K]	0.19	0.22	0.25	0.29	0.34
m_r	3.16	3.43	3.72	4.23	4.99
ϵ_D	0.98	0.97	0.96	0.96	0.96
ϵ_H	0.95	0.93	0.91	0.89	0.86
T_{min} [K]	303.15	303.15	303.15	303.15	303.15
T_{max} [K]	341.11	343.16	345.03	348.54	352.99

Table 7: OAOW-AH optimization results as a function of the minimum terminal temperature difference in either the humidifier or the dehumidifier, $\phi_{in} = 0.6$.

	Minimum Terminal Temperature Difference			
Parameter	2 K	3 K	4 K	5 K
GOR	3.26	1.82	0.98	0.41
s_{gen} [kW/K]	0.37	0.62	1.11	2.49
m_r	1.43	1.01	0.67	0.40
ϵ_D	0.96	0.92	0.85	0.83
ϵ_H	0.95	0.93	0.92	0.92
T_{min} [K]	303.15	303.15	303.15	303.15
T_{max} [K]	370.15	370.15	370.15	370.15